Available online at www.sciencedirect.com
ScienceDirect
Magnetic Resonance Imaging 27 (2009) 1011 – 1018
MAGNETIC RESONANCE IMAGING

Research articles

Investigation of high-resolution functional magnetic resonance imaging by means of surface and array radiofrequency coils at 7 T☆

Wietske van der Zwaag [a,b,*], José P. Marques [a,b], Martin Hergt [a,c], Rolf Gruetter [a,b,d]

[a]Laboratory for Functional and Metabolic Imaging, Ecole Polytechnique Fédérale de Lausanne, Lausanne, 1015 Switzerland
[b]Department of Radiology, University of Lausanne, Lausanne, 1015 Switzerland
[c]Siemens Switzerland, Healthcare Sector, Lausanne, Lausanne, 1015 Switzerland
[d]Department of Radiology, University of Geneva, Geneva, 1015 Switzerland

Received 18 October 2008; revised 8 January 2009; accepted 9 January 2009

Abstract

In this investigation, high-resolution, 1×1×1-mm^3 functional magnetic resonance imaging (fMRI) at 7 T is performed using a multichannel array head coil and a surface coil approach. Scan geometry was optimized for each coil separately to exploit the strengths of both coils. Acquisitions with the surface coil focused on partial brain coverage, while whole-brain coverage fMRI experiments were performed with the array head coil. BOLD sensitivity in the occipital lobe was found to be higher with the surface coil than with the head array, suggesting that restriction of signal detection to the area of interest may be beneficial for localized activation studies.

Performing independent component analysis (ICA) decomposition of the fMRI data, we consistently detected BOLD signal changes and resting state networks. In the surface coil data, a small negative BOLD response could be detected in these resting state network areas. Also in the data acquired with the surface coil, two distinct components of the positive BOLD signal were consistently observed. These two components were tentatively assigned to tissue and venous signal changes.

Keywords: High resolution; fMRI; Ultra high field; ICA

1. Introduction

High-resolution functional magnetic resonance imaging (fMRI) is becoming more widely available with the increasing numbers of high-field scanners and the advent of parallel imaging. The improved sensitivity of the method at higher magnetic fields stems from the nature of the BOLD signal, which is based on changes in concentration of deoxyhemoglobin, a paramagnetic agent, during brain activation. As the concentration of deoxyhemoglobin drops, the susceptibility difference between the veins or venules and the surrounding tissue changes and signal loss due to T2* effects is reduced [1]. This is seen as a signal increase in T2*-weighted MR images such as those acquired with EPI. Recently, it has been shown [2–5] that the susceptibility-induced signal change increases with increasing field strength. Thus, BOLD signal changes are larger at higher fields. In addition, the high field provides higher SNR. Consequently, fMRI acquisitions at higher fields can be performed with improved spatial resolution. Furthermore, the short venous T2* at high field strengths compared to the tissue T2* [6] reduces the intravenous contribution to the BOLD signal and thus improves the spatial specificity to detect activated tissue vs. larger vessels and veins [5,7,8]. High spatial resolution also allows for an identification of veins as they show up as areas of low signal intensity in the underlying EPI image. This vastly improved sensitivity of BOLD fMRI at higher field strengths opens the perspective of high-resolution fMRI, here defined as having a voxel size below 2 mm^3 [9].

On the other hand, susceptibility-induced distortions, through-slice gradient-induced signal drop-outs in the frontal lobes and near the inner ear, and physiological noise [10,11] scale with the magnetic field strength and

☆ This work was supported by Centre d'Imagerie BioMédicale (CIBM) of the UNIL, UNIGE, HUG, CHUV, EPFL and the Leenaards and Jeantet Foundations and the SNF grant 3100A0-116220.

* Corresponding author. CIBM, EPFL, Station 6, CH-1015 Lausanne, Switzerland. Tel.: +41 21 6937687; fax: +41 21 6937960.
E-mail addresses: wietske.vanderzwaag@epfl.ch, wietskez@gmail.com (W. van der Zwaag).

0730-725X/$ – see front matter © 2009 Elsevier Inc. All rights reserved.
doi:10.1016/j.mri.2009.01.013

are correspondingly increased at 7 T. These effects, however, can be compensated by reduced slice thickness and high gradient amplitudes and slewrates [12], as used in high-resolution EPI acquisitions. Increasing the resolution of fMRI may further be beneficial, as the physiological noise component decreases relative to thermal noise [13,14].

To attain high spatial resolution, a large imaging matrix has to be acquired in a short period of time. Assuming good shimming, the optimum TE for BOLD fMRI is approximately 28 ms at 7 T [6], which allows for an acquisition time of around 50 ms for a symmetrically sampled *k*-space matrix. For matrix sizes which can be as large as 192 phase-encoding lines, this can be achieved with a combination of strong gradients and partial *k*-space acquisition strategies such as parallel imaging. High image resolution can otherwise be reached through partial brain coverage using outer volume suppression or zoomed EPI [15].

With the use of those techniques, previous high-resolution fMRI studies at 7 T observed the ocular dominance columns [16] ($0.5\times0.5\times3\text{-mm}^3$ resolution) and orientation columns [17] ($0.5\times0.5\times3\text{-mm}^3$ resolution) in the visual cortex or demonstrated somatotopic mapping in the motor cortex [18] (1.5×1.5×2-mm resolution) and in subcortical regions [19] (1.4×1.4×1.5-mm resolution) with a maze-solving task [20] (1.46×1.46×2-mm resolution). Interestingly, submillimeter resolution was only reported in those 7-T studies employing partial brain coverage.

Isotropic or quasi-isotropic voxels allow for a more accurate estimate of active regions [20], but it is difficult to cover the entire brain in the *z*-dimension with a reasonable TR and TE without the possibility of acceleration in the *z*-dimension. This requires a receive array coil with a very high number of coils combined with either a 3D readout [21] or a multi-slice selection approach which provides additional speed-up factors in the slice-select direction [22]. Another strategy restricts the

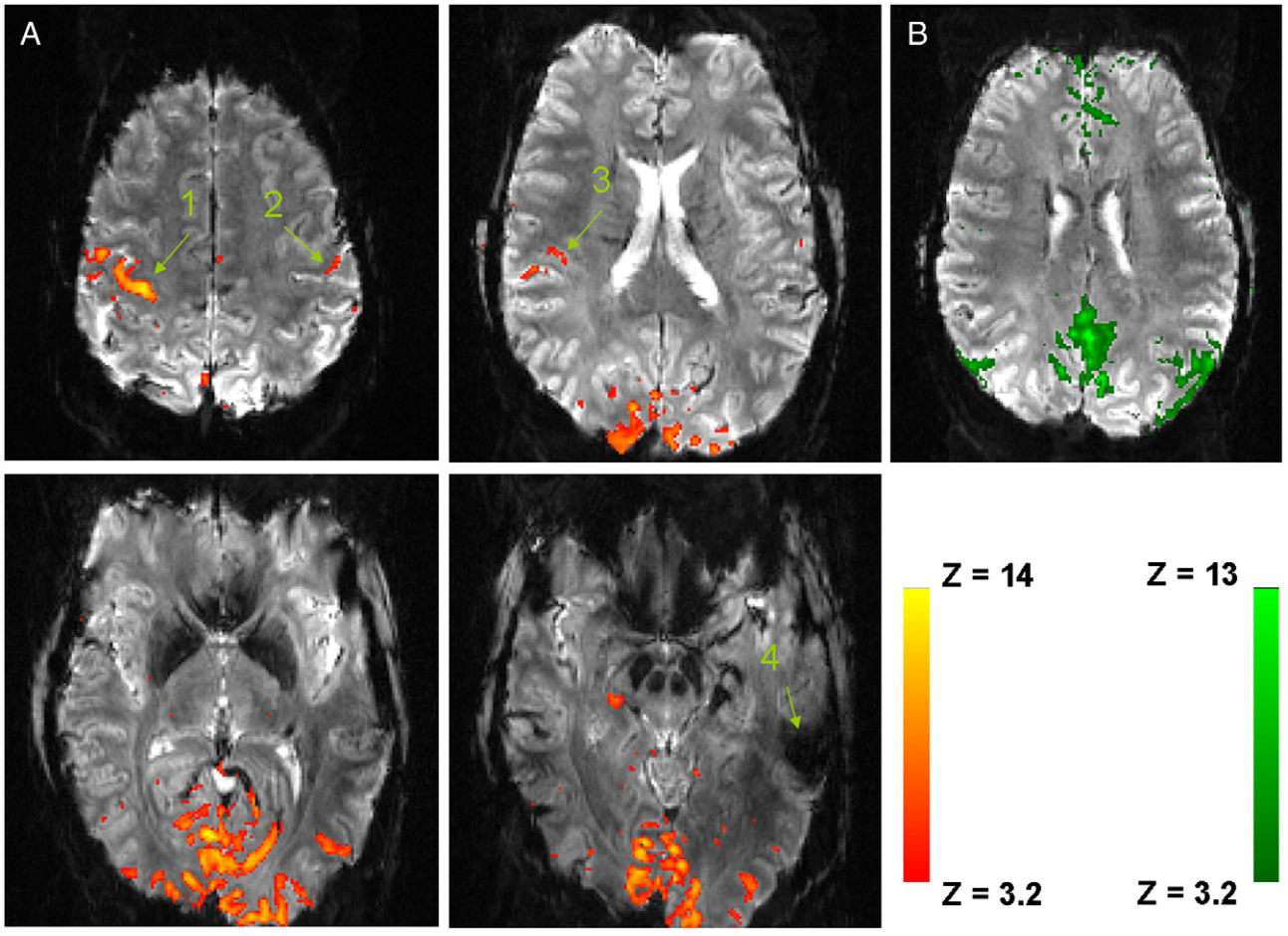

Fig. 1. (A) *Z*-score maps (thresholded at $Z>3.2$) from eight-channel coil data. Selected slices from a representative subject are shown. Note the good spatial correlation between the gray matter bands and the active areas. (1) Contralateral primary motor cortex, (2) ipsilateral primary motor cortex, (3) secondary somatosensory cortex and (4) area with signal drop-out due to through-slice dephasing near the inner ear. (B) Spatial representation of an ICA component of the same data shown in (A) assigned to the default network. Again good spatial correlation between the gray matter areas and the BOLD fluctuations is found.

FOV to the area of interest: with a suitable surface coil and possibly the use of a zoomed version of EPI [15], many regions of interest (ROIs) for fMRI can be reached and adequately scanned.

In this study, we explored the possibilities of performing high-resolution fMRI by means of surface and array radiofrequency (RF) coils at ultrahigh field, taking advantage of the strengths of each of these coils. The aim of the study was to (a) show that high-resolution fMRI is possible even if parallel imaging techniques are not available, (b) provide an initial evaluation of the benefits of high-resolution fMRI and (c) show that venous and tissue components of the BOLD signal can be identified using independent component analysis (ICA) decomposition of high-resolution fMRI data. To optimally show the strengths of each of the coils and to avoid a bias of the results towards one coil or the other, the scan parameters in terms of geometry were optimized for each coil separately.

2. Methods

In this investigation 12 subjects were scanned. Two sets of high-resolution fMRI experiments were performed: one based on whole-head coverage using a commercially available eight-channel head array coil (RAPID Biomedical GmbH, Germany) and the second using a surface coil and partial brain coverage. Permission for the study had been obtained from the local ethics committee and all subjects provided written informed consent.

All data was acquired using a human 7-T/680-mm scanner (Siemens Medical Solutions, Erlangen, Germany) equipped with a gradient insert coil (G_{max}=80 mT/m, G_{slew}=400 T/m per second). The stimulus was presented on a screen covering the back of the magnet bore and observed via a pair of prism glasses providing a viewing angle of ±25°.

Shimming was performed using the manufacturer's routine, the outcome was always visually evaluated and the routine was repeated until a satisfactory shim quality was reached. The area over which was shimmed corresponded to the area covered by the imaging slices.

Five subjects (four female, one male) were scanned with the eight-channel head array coil. Volumes acquired with the array coil consisted of 50 AC-PC aligned slices with a matrix size of 192×192 and a slice gap of 1 mm. This ensured whole-brain coverage for all subjects with a resolution of 1×1×2 mm^3. Other scan parameters were TE=28 ms, TR=2500 ms, flip angle=80°, partial *k*-space acquisition factor 6/8, GRAPPA factor 2. A short TR was chosen to demonstrate that high spatial resolution can be obtained without compromising temporal resolution.

The activation paradigm employed an 8-Hz black-and-white flashing checkerboard for visual stimulation, with the following timings: 10 s ON–20.5 s OFF, N=10. To elicit activation in multiple brain regions, subjects were asked to tap their left index finger as fast as possible while the checkerboard was flashing. The flashing checkerboard served as a visual cue as well as a stimulus. Offline motion correction showed that none of the subjects displayed an unacceptable level of motion (mean displacement <1 mm) and all data was used for further processing.

Seven different subjects (four female, three male) were scanned with a home-built quadrature surface coil. This design consists of two 13-cm-diameter loops [23] and provides excellent coverage of the occipital lobe. The local SNR of the surface coil matched that of the array coil at a distance of approximately 9 cm from the scull, easily sufficient to cover the entire occipital lobe of a typical volunteer.

Volumes acquired with the surface coil consisted of 25 coronal slices with isotropic voxel size of 1×1×1 mm^3 (128×128 matrix) and a slice gap of 0.1 mm, covering the visual cortex. Slices were placed to cover as much of the occipital lobe as possible, with the sagittal sinus as the posterior limit. For the comparison, we employed identical

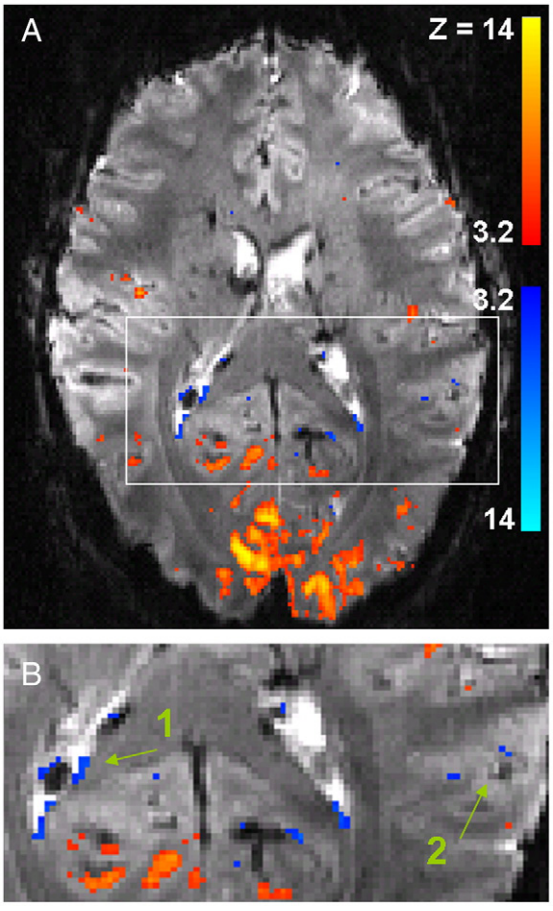

Fig. 2. Example activation map from whole-brain data shown overlaid on one of the volumes of the acquisition train. Positive correlation is shown red-yellow, negative correlation in blue. The area outlined in (A) is shown enlarged in (B). Arrows in (B) indicate areas which display negative BOLD signal near the posterior end of the ventricals (1) and in veins found in the cortical folds (2).

parameters in both sets of experiments (TR/TE/α and partial *k*-space acquisition factor: 2500 ms/28 ms/80°/6/8). As the area of interest was smaller than for the array coil experiments, the data could be acquired with thinner slices and a smaller FOV. The paradigm employed consisted of the same black-and-white checkerboard as that employed for the array coil experiments, but this time subjects were not asked to perform a motor task. One subject was excluded from further processing due to excessive motion (mean displacement >1 mm).

2.1. Data processing

All data were realigned, corrected for slice timing errors, temporally filtered and spatially smoothed with a Gaussian of FWHM 1.5 mm. This relatively small width of the Gaussian was chosen to retain the high spatial resolution. *Z*-score maps, thresholded at a corrected *p* factor of 0.05, were obtained using FEAT from FSL (FMRIB's Software Library). Independent component analysis was performed using MELODIC [24] from FSL.

To demonstrate the effect of reduced spatial resolution, the surface coil data was also processed after down sampling in image space to a resolution of 3×3×2 mm^3. This down-sampled data was subjected to the same processing as the high-resolution data, with the exception that the spatial smoothing was done with a Gaussian of FWHM 4.5 mm.

It is possible to reduce distortions with the use of a separately acquired fieldmap [25], but as the cortical ribbons are clearly visible in high-resolution echo planar images [12] and the use of fieldmaps may result in image artifacts [26], it was decided to omit the fieldmap distortion correction from the data-processing chain.

Identification of components from the MELODIC analysis related to the early/late BOLD response, physiological noise and resting state networks was done by visual inspection. Those components which displayed continuous areas (≥6 cm^3) of coherent voxels within the brain, with a time course unrelated to the stimulus paradigm, were regarded as resting state networks.

For each subject, ROIs were drawn by hand in the primary motor and visual cortex of the whole-brain data. These were subsequently combined with the activation mask to obtain ROIs of activation in the visual and primary motor cortex. For all subjects, percentage change maps were calculated from the reordered activation time courses whereby the ON period was defined as the mean signal intensity between 5 and 12.5 s after stimulus onset and the OFF period was defined as the time between 10 and 17.5 s after stimulus end.

The time courses from active ROIs were reordered according to their temporal delay with respect to stimulus onset to allow the graphical depiction of the local hemodynamic response function (hrf) with a temporal

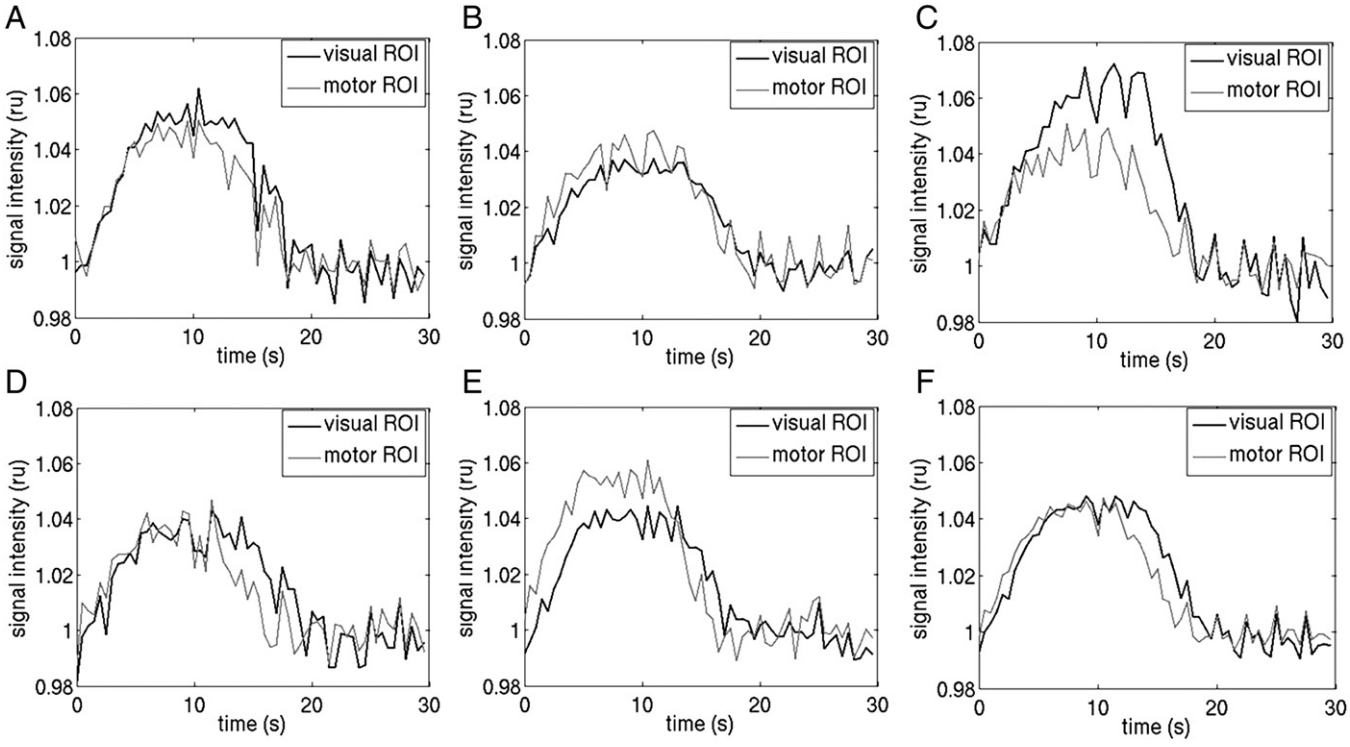

Fig. 3. Time courses obtained from active ROIs per subject (A–E) and as mean over subjects (F) Time course data were reordered with respect to the stimulus onset to improve hrf definition.

resolution of 500 ms. To improve the long-term stability of the time courses for hrf analysis, the first eight components of the ICA decomposition identified as artifacts, motion, physiological noise or other noise-like signals were removed using a routine provided by MELODIC [24,27] before reordering the volumes.

3. Results

3.1. Array coil

During simultaneous motor and visual stimulation, activation of the contralateral M1/S1, contra- and ipsilateral S2, SMA and lower brain regions was consistently detected using the GLM approach (Fig. 1A) as well as ICA decomposition. Resting state networks as described in the literature [28] were found in all subjects using ICA, the most predominant was the default mode network (Fig. 1B), but the auditory system and lateral visual cortex networks were also found.

Correlations with an inverted hrf were found in small, focal locations throughout the brain including the frontal lobes (Fig. 2), presumably originating in veins. Negative BOLD activation was consistently found near the occipital horns of the ventricles.

The averaged signal intensity time courses from the visual and motor cortex ROIs are shown for each subject in Fig. 3A–E. For all five subjects, the shape of the hrf in the motor cortex was different from the hrf in the visual cortex while subject-to-subject variation was also evident (Fig. 3). For example, differences in BOLD amplitude, time-to-peak, hrf duration and presence of post-stimulus undershoot are discernable in Fig. 3. For two subjects, the onset of the hrf in the motor cortex significantly preceded that of the visual cortex. For the other three subjects, an almost simultaneous onset of the BOLD response was found in the visual and

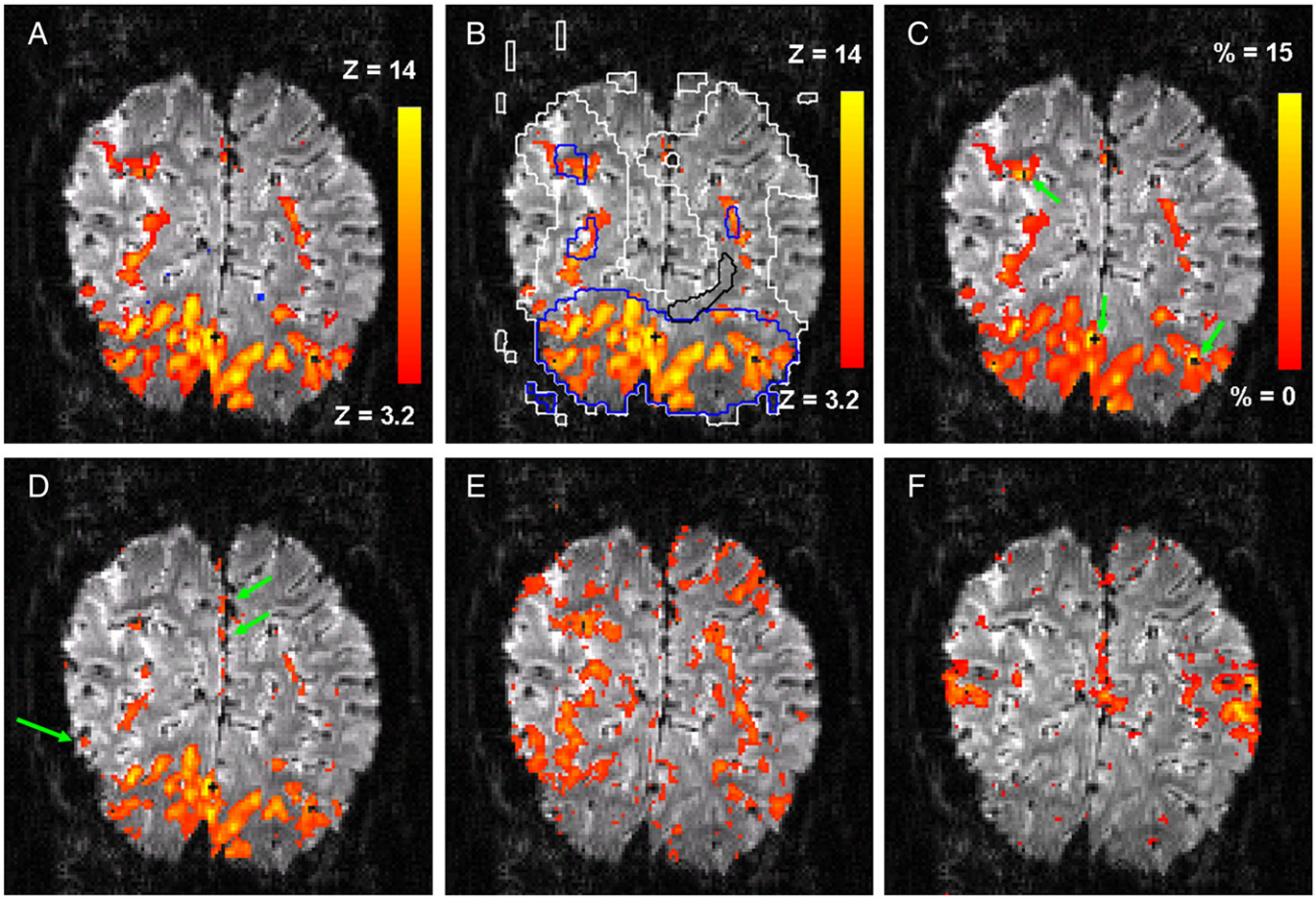

Fig. 4. Slices taken from a representative dataset acquired with the surface coil; all maps are shown overlaid on a volume of the fMRI acquisition train. (A) *Z*-score map. Positive correlations are shown in red-yellow, negative correlation is shown in blue. (B) Activation maps shown with and without down sampling of the data; the activation map obtained from the down sampled data is shown with white and blue outlines. The white isobar indicates z=4; the blue isobar, z=8. A white matter ROI is shown in black. (C) % change map. (D) Component 1 from the ICA decomposition. Arrows point out veins which were not shown to be active in the *z*-score map. (E) Component 5 from the ICA decomposition. (F) Component 12 from the ICA decomposition, tentatively assigned to the visuo-spatial resting state network.

motor areas. For all subjects, the hrf was shorter in duration in the motor cortex than in the visual cortex; this can also be seen in the mean hrf over subjects (Fig. 3F).

The BOLD signal change averaged over all subjects in both the motor and visual cortex was 5% (Fig. 3F). The average size of the active ROIs was 21±0.2 cm^3 (mean±S.E.). Individual voxels displayed signal changes of up to 25–30%. In general, the visual cortex displayed a 10 times larger area of activation than the motor cortex (1.9±0.1 cm^3).

3.2. Surface coil

Fig. 4A–E shows a representative activation map from one slice in one subject but with various analysis approaches. Activation (p_{corr}<0.05) was consistently detected using a GLM or ICA approach. Positive BOLD signal showed excellent spatial correlation with the cortical gray matter (Fig. 4A). Negative BOLD was also detected, located in draining veins at some distance from the primary visual cortex (Fig. 4A). The SPM obtained from the down-sampled data for the same subject is shown overlaid with contour lines at z=4 and z=8 for comparison with the high-resolution activation map (Fig. 4B). In the low-resolution data, 'activation' was found in a large area including white matter tissue and even when a higher z-score threshold (z=8) was applied, white matter was still included in the active mask. For example, the ROI shown in black in Fig. 4B contains mainly white matter. The average z-score found over this white-matter ROI from the down-sampled data was 5.6 and the average BOLD signal change over the ROI in the down-sampled, smoothed data is 0.6%. However, in the same dataset, in the same ROI, without down sampling and after smoothing with a 1.5-mm FWHM kernel, a signal change of −1.3% was found. This means that any activation found in this particular ROI in the low-resolution data was likely a result of 'smoothing in' from surrounding tissue and neighboring slices and not related to physiological activation.

The percentage change map obtained from the high-resolution data shown in Fig. 4A is shown in Fig. 4C; arrows indicate areas identified as draining veins from the low signal intensity in the underlying echo planar image. In the percentage change map, dramatic increases in BOLD signal change were observed at these locations, reaching values as high as 40%. The average signal change in the visual cortex was 4±1% (subjects mean±S.D.) over an area of 23±7 cm^3. Time courses extracted from the active ROI and the voxel with the maximum z-score from a representative subject are shown in Fig. 5A. It is noteworthy that the SNR of the time course of a single 1×1×1-mm^3 voxel was sufficient for hrf characterization.

The first component in the ICA decomposition, which is the one that explains the largest amount of variance, was for all subjects activation related. Delayed or early components, associated with venous and tissue areas, respectively, were found in all but one subject, as illustrated by the spatial representations of the first (Fig. 4D) and fifth (Fig. 4E) components from the ICA decomposition of a representative dataset. Both components have good spatial correlation with the z-score map as well as a correlation of the associated time course with the hrf (Fig. 5B). Component 1 was somewhat delayed relative to Component 5, suggesting a location closer to draining veins as also implied from their spatial localization with respect to veins in the underlying image (Fig. 4D–E).

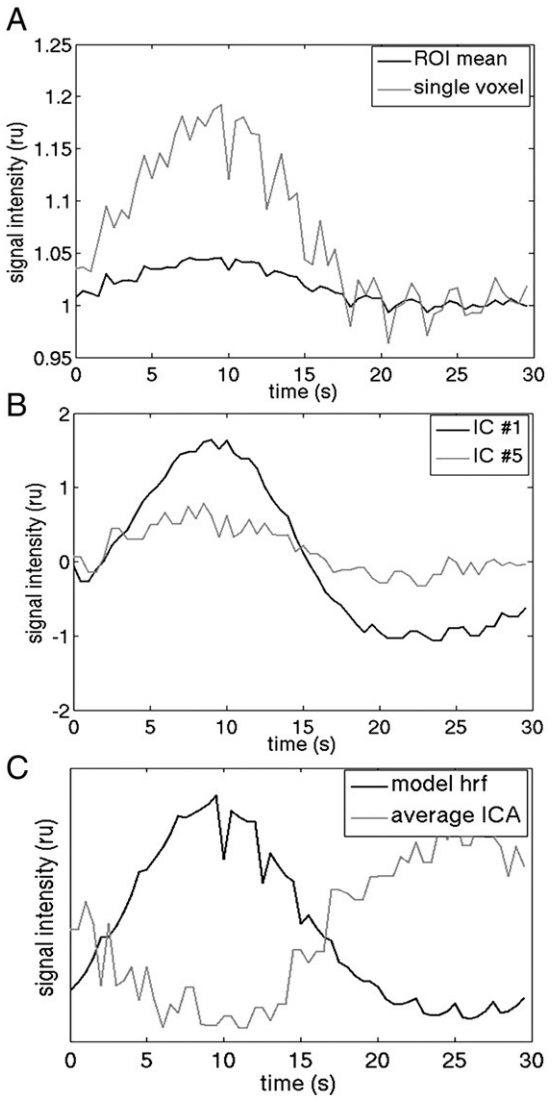

Fig. 5. Signal time courses taken from surface coil data of a representative subject. (A) Reordered time courses from the ROI average and the voxel with the maximum z-score. The mean BOLD signal change here was 4.3%. (B) Reordered time courses associated with the independent components shown in Fig. 4C and D. A median filter of width 4 has been applied to reduce cycle-to-cycle variation. (C) The hrf model function is shown in black after reordering of the data points. Anticorrelation with the mean-over-subjects time course from a resting state network shown in gray is visible. A median filter of width 4 has been applied to the ICA time course to reduce cycle-to-cycle variation.

A resting state network in the occipital lobe, tentatively identified as the visuo-spatial network, was detected in all subjects (Fig. 4F). The mean-over-subjects time courses associated with this component was anticorrelated (z=5.0) with the activation paradigm (Fig. 5C).

4. Discussion

Good image quality was achieved in high-resolution echo planar images at 7 T using an optimized EPI sequence with sinusoidal gradient waveform [12], optimal TE for BOLD fMRI and limited acquisition time. Processing of the data revealed activation limited to gray matter structures (Figs. 1 and 4A). However, when data was down sampled to a commonly used voxel size of 3 mm, 'activation' was also found in white matter areas (Fig. 4B, contour lines) even when in the high-resolution data a small, negative BOLD signal was found in the same ROI. This result indicates that partial volume effects decrease the spatial specificity of the BOLD method in typical applied fMRI protocols at 1.5 or 3 T. In other words, these results underlie the importance of improving spatial resolution in fMRI experiments that rely on high spatial specificity.

4.1. Acquisition strategies

For high-resolution BOLD fMRI with whole-brain coverage, array coil technology and parallel imaging are required to maintain BOLD contrast without reducing spatial and/or temporal resolution. Even with the eight-channel coil and relatively short readout duration, a slice thickness of ~2 mm is needed for full brain coverage in 2.5 s. This resulted in through-slice signal dropout near the inner ear (Fig. 1) and in the frontal areas, which are of high importance in neuroscience experiments. While distortions can be corrected [29] or prevented by even shorter readout trains, through-slice signal de-phasing leads to irreversible signal loss. This signal can be acquired in a separate acquisition [30], but this increases the effective TR.

As an alternative approach, partial brain, thin-sliced, high-resolution BOLD fMRI may also be obtained with surface coils, which may be particularly beneficial if a well-defined area is to be studied. Another important advantage of the use of surface rather than array coils is the lower SAR level. On the other hand, the inhomogeneity of the B1 profiles within the ROI may be disadvantageous.

Of the two experimental setups shown here, the surface coil data appeared to yield a slightly higher BOLD sensitivity in the occipital lobe: a similar volume of active brain tissue was found, using a smaller voxel size and all other parameters including the paradigm and TE kept constant, while at this spatial resolution, a reduction in voxel size is expected to result in a smaller detected active volume [12]. Furthermore, in the ICA decomposition of the surface coil data, the main BOLD component was always the most important ICA result, and for all but one subject a second, distinct, BOLD-related component was found within the first 10 components. For the array coil, only in two of five subjects was the BOLD component the most important independent component. This difference is likely due to the larger number of voxels in the array data; the active tissue covers a smaller subset of the volume in the array coil data than in the surface coil data. This confirms that it may be beneficial, if the location of the expected activation is known, to reduce the brain volume scanned during fMRI data acquisition, either through the use of a surface coil or through selective use of individual loops in an array RF coil. These strategies can be used either with or without outer volume suppression [15,16].

4.2. Post-processing strategies

ICA analysis could be used to distinguish 'tissue' and 'venous' components to the BOLD signal in the surface coil data; while the temporal SNR of the tissue component 5 (Fig. 5B) was low, it was sufficient to notice several differences relative to the venous component: a reduction in BOLD signal amplitude, a shift in time-to-peak and the absence of a marked BOLD undershoot. All these suggest that Component 5 is more tissue related than Component 1. While the BOLD undershoot especially is typically better studied with a longer inter-stimulus interval, it is clear that the SNR of an experiment as the one presented here is high enough to study differences in hrf shape such as duration and onset.

Inter-subject variability in hrf amplitude and shape was evident (Fig. 3). The differences in hrf shapes found in different subjects and/or brain areas most likely reflect differences in local perfusion. Both the onset and return to baseline of the hrf were faster in the motor cortex, possibly because the motor cortex covers a smaller volume than the visual cortex.

The data shown in Fig. 4C illlustrate a possible way to identify draining veins in high-resolution fMRI data. As shown before [4,5], if the spatial resolution is high enough, identification can be done by simply selecting focal low-intensity areas in the underlying EPI data which are surrounded by high % BOLD change. According to the data shown here, a local high % BOLD signal change is a better indicator of veins than a local high z-score.

Negative BOLD signal was observed in this study and consistently colocalized to vessels. Subject motion could also result in negative BOLD contrast, but is unlikely to be a cause here because of the minimal bulk motion effects found in the data. Furthermore, apparent activation due to bulk motion along high-contrast structure often consists of both positive and negative 'BOLD' signal found on opposite sides of the structure, which is not the case here. Therefore, this localized negative BOLD signal implicates a hemodynamic effect rather than widespread neuronal deactivation or motion-induced artifacts.

The negative correlation between the time course of the visuo-spatial network and the model hrf (Fig. 5C) is likely due to a reduction of activity in the resting state network

during the active phase of the paradigm. That the negative correlation seen between the visuo-spatial resting state network found in the surface coil data and the hrf does not result in negative BOLD activation in the area of the resting state network is likely due to SNR limitations. The correlation was only significant when averaged over all subjects.

A challenge presented by high-resolution data is the large subject-to-subject variation in brain architecture at the length scales considered here. For group studies, a standard normalization procedure would incur considerable smoothing so that the high spatial resolution would be lost. An alternative is to normalize along the cortex, where the spatial resolution would be better retained [31].

5. Conclusion

We conclude that unless whole-brain coverage is essential for a given fMRI experiment, a surface coil offers a very good approach for the acquisition of high-resolution fMRI. In the data shown here for the occipital cortex, the sensitivity of the surface coil was slightly higher than that of the array coil. It is also shown that high resolution in fMRI is essential to correctly ascribe activation to gray matter tissue.

Acknowledgments

We thank Dr. Gunnar Krüger for useful contributions to this manuscript.

References

[1] Ogawa S, Lee TM, Kay AR, Tank DW. Brain magnetic resonance imaging with contrast dependent on blood oxygenation. Proc Natl Acad Sci U S A 1990;87(24):9868–72.
[2] Schafer A, van der Zwaag W, Francis ST, Head KE, Gowland PA, Bowtell RW. High resolution SE-fMRI in humans at 3 and 7 T using a motor task. MAGMA 2008;21(1-2):113–20.
[3] Fera F, Yongbi MN, van Gelderen P, Frank JA, Mattay VS, Duyn JH. EPI-BOLD fMRI of human motor cortex at 1.5 T and 3.0 T: sensitivity dependence on echo time and acquisition bandwidth. J Magn Reson Imaging 2004;19(1):19–26.
[4] Gati JS, Menon RS, Ugurbil K, Rutt BK. Experimental determination of the BOLD field strength dependence in vessels and tissue. Magn Reson Med 1997;38(2):296–302.
[5] Yacoub E, Shmuel A, Pfeuffer J, Van De Moortele PF, Adriany G, Andersen P, et al. Imaging brain function in humans at 7 tesla. Magn Reson Med 2001;45(4):588–94.
[6] Peters AM, Brookes MJ, Hoogenraad FG, Gowland PA, Francis ST, Morris PG, et al. T2* measurements in human brain at 1.5, 3 and 7 T. Magn Reson Imaging 2007;25(6):748–53.
[7] Menon RS. Postacquisition suppression of large-vessel BOLD signals in high-resolution fMRI. Magn Reson Med 2002;47(1):1–9.
[8] Menon RS, Ogawa S, Tank DW, Ugurbil K. Tesla gradient recalled echo characteristics of photic stimulation-induced signal changes in the human primary visual cortex. Magn Reson Med 1993;30(3):380–6.
[9] Kriegeskorte N, Bandettini P. Analyzing for information, not activation, to exploit high-resolution fMRI. NeuroImage 2007;38(4):649–62.
[10] Glover GH, Li TQ, Ress D. Image-based method for retrospective correction of physiological motion effects in fMRI: RETROICOR. Magn Reson Med 2000;44(1):162–7.
[11] Triantafyllou C, Hoge RD, Krueger G, Wiggins CJ, Potthast A, Wiggins GC, et al. Comparison of physiological noise at 1.5 T, 3 T and 7 T and optimization of fMRI acquisition parameters. NeuroImage 2005;26(1):243–50.
[12] Speck O, Stadler J, Zaitsev M. High resolution single-shot EPI at 7T. Magma 2008;21(1-2):73–86.
[13] Kruger G, Glover GH. Physiological noise in oxygenation-sensitive magnetic resonance imaging. Magn Reson Med 2001;46(4):631–7.
[14] Kruger G, Kastrup A, Glover GH. Neuroimaging at 1.5 T and 3.0 T: comparison of oxygenation-sensitive magnetic resonance imaging. Magn Reson Med 2001;45(4):595–604.
[15] Pfeuffer J, van de Moortele PF, Yacoub E, Shmuel A, Adriany G, Andersen P, et al. Zoomed functional imaging in the human brain at 7 Tesla with simultaneous high spatial and high temporal resolution. NeuroImage 2002;17(1):272–86.
[16] Yacoub E, Shmuel A, Logothetis N, Ugurbil K. Robust detection of ocular dominance columns in humans using Hahn spin echo BOLD functional MRI at 7 Tesla. NeuroImage 2007;37(4):1161–77.
[17] Yacoub E, Harel N, Ugurbil K. High-field fMRI unveils orientation columns in humans. Proc Natl Acad Sci U S A 2008;105(30):10607–12.
[18] Meier JD, Aflalo TN, Kastner S, Graziano MS. Complex organization of human primary motor cortex: a high resolution fMRI study. J Neurophysiol 2008;100(4):1800–12.
[19] Walter M, Stadler J, Tempelmann C, Speck O, Northoff G. High resolution fMRI of subcortical regions during visual erotic stimulation at 7 T. Magma 2008;21(1-2):103–11.
[20] Jerde TA, Lewis SM, Goerke U, Gourtzelidis P, Tzagarakis C, Lynch J, Moeller S, Van de Moortele PF, Adriany G, Trangle J, et al. Ultra-high field parallel imaging of the superior parietal lobule during mental maze solving. Exp Brain Res 2008;187(4):551–61.
[21] van der Zwaag W, Francis S, Bowtell R. Improved echo volumar imaging (EVI) for functional MRI. Magn Reson Med 2006;56(6):1320–7.
[22] Wu EL, Kuo LW, Wu FH, Hsu CF, Hsieh CW, Chen JH, et al. Ultra-fast brain MR imaging using simultaneous multi-slice acquisition (SMA) technique. Conf Proc IEEE Eng Med Biol Soc 2007;2007:2618–21.
[23] Cohen LG, Roth BJ, Nilsson J, Dang N, Panizza M, Bandinelli S, et al. Effects of coil design on delivery of focal magnetic stimulation. Technical considerations. Electroencephalogr Clin Neurophysiol 1990;75(4):350–7.
[24] Beckmann CF, Smith SM. Probabilistic independent component analysis for functional magnetic resonance imaging. IEEE Trans Med Imaging 2004;23(2):137–52.
[25] Jezzard P, Balaban RS. Correction for geometric distortion in echo planar images from B0 field variations. Magn Reson Med 1995;34(1):65–73.
[26] Zeng H, Constable RT. Image distortion correction in EPI: comparison of field mapping with point spread function mapping. Magn Reson Med 2002;48(1):137–46.
[27] Beckmann CF, Noble J, Smith SM. Artifact detection in FMRI data using independent component analysis. NeuroImage 2000;11:614.
[28] Damoiseaux JS, Rombouts SA, Barkhof F, Scheltens P, Stam CJ, Smith SM, et al. Consistent resting-state networks across healthy subjects. Proc Natl Acad Sci U S A 2006;103(37):13848–53.
[29] Zaitsev M, Hennig J, Speck O. Point spread function mapping with parallel imaging techniques and high acceleration factors: fast, robust, and flexible method for echo-planar imaging distortion correction. Magn Reson Med 2004;52(5):1156–66.
[30] Constable RT, Spencer DD. Composite image formation in *z*-shimmed functional MR imaging. Magn Reson Med 1999;42(1):110–7.
[31] Fischl B, Sereno MI, Tootell RB, Dale AM. High-resolution intersubject averaging and a coordinate system for the cortical surface. Hum Brain Mapp 1999;8(4):272–84.